Published in final edited form as:
Conf Proc IEEE Eng Med Biol Soc. 2011 ; 2011: 7787–7790. doi:10.1109/IEMBS.2011.6091919.

EMCCD-Based High Resolution Dynamic X-Ray Detector for Neurovascular Interventions

P. Sharma [Student Member, IEEE], **S.N. Swetadri Vasan [Student Member, IEEE]**, **A. Jain [Student Member, IEEE]**, **A. Panse [Student Member, IEEE]**, **A.H. Titus [Senior Member, IEEE]**, **A. N. Cartwright [Senior Member, IEEE]**, **D. R Bednarek**, and **S. Rudin [Life Member, IEEE]**
Electrical Engineering Department and Toshiba Stroke Research Center at University at Buffalo, The State University of New York, Buffalo, NY 14260-1920, USA

Abstract

We have designed and developed from the discrete component level a high resolution dynamic detector for neurovascular interventions. The heart of the detector is a 1024 × 1024 pixel electron multiplying charge coupled device (EMCCD) with a pixel size of 13 × 13 μm^2, bonded to a fiber optic plate (FOP), and optically coupled to a 350 μm micro-columnar CsI(TI) scintillator via a 3.3:1 fiber optic taper (FOT). The detector provides x-ray images of 9 cycles/mm resolution at 15 frames/sec and real time live video at 30 frames/sec with binning at a lower resolution, both independent of gain applied to EMCCD, as needed for region-of-interest (ROI) image guidance during neurovascular interventions.

I. Introduction

Neuro-interventional treatment of vascular conditions is accomplished with micro-catheters that are inserted through the femoral artery and threaded through the major vessels to reach the brain. This enables a variety of treatments such as placing metallic coils in aneurysms to prevent rupture, opening up stenosed arteries with a stent, delivering clot-busting medication to open up arteries of stroke victims, and providing more accurate diagnostic angiographies. These minimally invasive procedures impose strict requirements on the imaging systems needed to guide the devices such as high resolution, high speed, high sensitivity and low readout noise.

Current medical x-ray imaging systems include x-ray image intensifiers (XII), flat panel detectors (FPD) and charge coupled device (CCD) based detectors. While XII based detectors suffer from problems of veiling glare and image distortion such as pincushion or s-shaped distortions [1] due to the earth's magnetic field, the biggest limitation of both XIIs and FPDs is their limited spatial resolution of approximately 2–3 cycles/mm. A new CCD-light-image-intensifier-based x-ray detector the Micro-Angiographic Fluoroscope (MAF) [2] being developed by our group at the UB-TSRC provides exceptional performance in terms of resolution, speed and sensitivity but requires a high voltage above 1000V. Moreover, the field of view (FOV) of the MAF is not easily extensible.

To overcome all these limitations we have designed and developed from the discrete component level a high resolution dynamic EMCCD-based x-ray detector. This detector's FOV is readily expanded by the use of an array of EMCCD based modules [3].

The corresponding author is P. Sharma, phone: 716-829-5417; psharma4@buffalo.edu.

II. DESIGN AND CONSTRUCTION

A. Detector

As shown in Fig. 1 the detector includes an EMCCD sensor optically bonded to a fiber optic plate which is optically coupled to micro columnar scintillator phosphor CsI(TI) using a fiber optic taper.

1) EMCCD Sensor—The heart of the detector is a back-illuminated L3Vision™ EMCCD sensor (CCD201-20) manufactured by e2v Technologies Ltd, UK [4]. It consists of 1024×1024 active image pixels, each 13 μm × 13 μm in size providing an active image area of 13.3 × 13.3 mm^2.

As shown in Fig. 2, the EMCCD is similar to a frame-transfer CCD with the addition of a multiplication register stage; this stage requires the application of a voltage of 40–45V to cause avalanche multiplication of electrons through impact ionization. The probability of impact ionization or gain per stage is given by g providing a total gain of $M = g^N$ where N is the number of gain stages [5]. Since this signal amplification happens before the charge-to-voltage conversion in the output amplifier (this being the main source of readout noise), the effective signal is increased well above the noise floor [6]. Since the EMCCD is a back-illuminated sensor, it has a peak quantum efficiency of over 92% over the spectral response ranging from 500 to 600 nm.

2) Scintillator—A 350 μm thick structured cesium iodide CsI(TI) scintillator is used to convert the incoming x-ray photons into light photons. CsI(TI) has an effective atomic number of 54 resulting in good quantum detection efficiency over the medical x-ray energy range (20–140 kV). The emission spectral response of CsI ranges from 350 to 700 nm with peak near 565 nm [7] which matches with the EMCCD sensor.

3) Fiber Optic Tapers & Plates—The fiber optic plates (FOP) and a fiber optic taper (FOT) (Incom, Inc., Charlton, MA) is used to channel the light photons from the scintillator onto the EMCCD. A custom FOP [8] of dimension (15×15×5) mm is bonded using epoxy on the imaging region of the EMCCD. For initial testing, a FOT with magnification ratio of 3.3:1 is used to optically couple the FOP and the scintillator, providing an effective pixel size of 42.9 × 42.9 μm^2 (3.3 times the pixel size of EMCCD) which enables very high resolution for neurovascular features such as small perforated vessels, stenoses, and endovascular device structures such as stent struts.

B. Electronics

The electronics for the detector is constructed using discrete components and comprises two PCB boards: an analog front end (AFE) board to drive the EMCCD and a FPGA board to generate clocks for AFE. As shown in Fig. 3 the AFE board consists of the circuits to drive image area clocks, storage area clocks, serial register clocks and a special high voltage clock circuit used to provide a 0–50 volt sinusoidal clock at 17.5 MHz for electron multiplication using impact ionization. The AFE board also has a 12 bit CCD signal processor, VSP2562 (Texas Instruments, Inc., Dallas, TX), used to convert the EMCCD analog output into a 12 bit digital output. Layout of the AFE board is designed to minimize noise issues and ensure signal integrity. For example, analog and digital ground mixing was minimized, ringing in clocks was reduced using series RC terminations at the load and damping resistors at the source, and ground debounce was minimized by using appropriate capacitors.

The FPGA board using the XC3S100E-VQ100 (Xilinx, Inc., San Jose, CA) [9] FPGA is used to generate the clocks for the AFE board. It is programmed using verilog hardware

description language (VHDL) through proprietary programming software provided by Xilinx. A crystal oscillator of 280 MHz is used to provide the master clock to the FPGA. A minimum time slice of 3.57 ns was necessary to adjust delays in the clocks to achieve optimized output from the EMCCD sensor. A trigger input was also provided to the FPGA board which can be connected to the X-ray unit to get two modes of operation: triggered and continuous.

C. Data Acquisition

For acquiring the 12 bit digital output a CameraLink image acquisition board (NI PCIe-1430 from National Instruments, Inc.[10]) is used. The CameraLink standard provides a fast interface for high resolution and high speed cameras with data rate capabilities up to 2 Gbps. The FPGA board is connected to the NI board using a CameraLink cable as seen in Fig.4. The software platform LabVIEW (National Instruments, Austin, TX) is used to control the camera as well as acquire and process the images.

The experimental setup to test the prototype detector is shown in Fig. 5.

III. RESULTS & DISCUSSION

A. High Resolution

The pixel size of the sensor is $13 \times 13\ \mu m^2$ which gives a Nyquist frequency of 38 cycles/mm. The detector has three components, CsI(TI), FOT and FOP, before the sensor in the imaging chain and each of these components have their respective limitations on resolution [11,12,13] which produces a cascading effect that ultimately limits the resolution of the sensor. Fig. 6 shows an x-ray image of a line pair phantom taken at 50 kV and 1.2 mAs. The high resolution capability of the detector is readily observable. We can easily resolve 9 cycles/mm even after the degradation in resolution due to other components.

B. Linearity

Detector linearity indicates the relationship between input signal in terms of photons and the output signal in average digital numbers. Linearity is particularly important in quantitative imaging for ratio calculations, flat field corrections and to achieve a high dynamic range. Fig. 7 shows the linearity data for the detector at different detector entrance exposures. A standard RQA5 spectrum was used to calculate this curve.

C. Multiplication Gain

The effect of the multiplication gain is shown in the images in Fig. 8(a) (b) (c). Two different neurovascular stents were visualized: a thicker 120 μm strut stainless steel stent (below) and a thinner 100 μm strut nitinol stent (above). The technique parameters for the x-ray machine were 50kV, 100mA and 10ms. To achieve gains of 2x, 4x, and 10x, the high voltage multiplication clock of the sensor was increased from 39V which represents a gain of 1x to 41V, 42V and 43V respectively. The temperature of the detector while performing the preliminary tests was approximately 27°C, resulting in a very limited range of the multiplication gain. Higher gains can be achieved using more cooling.

D. No Secondary Quantum Sink

A desirable goal in terms of noise properties for an x-ray imaging system is that it should be x-ray quantum limited rather than limited at any other stage in the imaging chain. Such a secondary quantum sink may necessitate unnecessary additional radiation dose to the patient. Fig. 9 shows the quantum accounting diagram (QAD) for this detector in which the number of quanta at each stage in the imaging chain, calculated and measured from data, is

plotted. The average energy of the input x-ray is taken to be 54 keV. Stage 1 represents input x-ray quanta and starting with 1 x-ray photon. Stage 2 represents absorption of x-ray photons in the CsI(TI) with an absorption efficiency of 65%. Stage 3 represents conversion of x-ray photons to light photons in CsI(TI). Approximately 18 eV of x-ray energy is needed to produce one light photon and an absorbed x-ray of 54 keV produces about 3000 light photons of which 2100 leave the phosphor. Stages 4, 5 and 6 represent the FOP on the CsI(TI) phosphor, the FOT and the FOP on the sensor with respective transmission efficiencies of 60%, 18%, and 60%. Stage 7 represents the 92% quantum efficiency of the EMCCD which indicates 0.92 electrons are generated per light photon. The final stage is the multiplication gain. If the net gain for 604 multiplication stages were 50, the gain per stage would be 1.00649 using $M = g^N$ where N is the number of gain stages.[5]. To avoid any secondary quantum sink it is necessary that the number of quanta used along the imaging chain cannot be less than the number of detected x-ray quanta. We can clearly see from the QAD that there is no secondary quantum sink.

E. Cooling to achieve lower exposures

Due to the dark signal and thereby gain dependence on the temperature [14], cooling is necessary to achieve larger multiplication gains and thereby allowing us to operate at lower exposure ranges. Fig. 10 shows the linearity of the detector with cooling.

Comparing exposure ranges in Fig. 10 with Fig. 7 we can see that a sufficient cooling allows us to operate the detector at very low exposure ranges and higher gains. A single stage Peltier cooler was used for cooling the sensor and temperatures in the range of 5°C were recorded.

IV. CONCLUSION

In this paper we have presented a prototype design for an EMCCD based x-ray detector. The system is shown to have high resolution, linearity, variable multiplication gain and no secondary quantum sink. The current prototype detector has a field of view (FOV) of 4.2 × 4.2 cm^2. A 3×3 array of these detectors is currently being designed to achieve a larger FOV comparable with flat panel detectors. These properties make this detector ideal as the core of a neuro-endovascular imaging system.

Acknowledgments

This work is supported in part by NIH Grants R01-EB008425 and R01-EB002873, and an equipment grant from Toshiba Medical Systems Corp.

We also thank e2v Technologies Ltd, UK for providing us with technical assistance and EMCCD sensors.

References

1. Rudin S, Bednarek DR, Wong R. Accurate characterization of image intensifier distortion. Med Phys. 1991; 18(6):1145–1151. [PubMed: 1753896]
2. Rudin S, Wu Y, Kyprianou IS, Ionita CN, Wang Zhou, Ganguly A, Bednarek DR. Micro-angiographic detector with fluoroscopic capability. Proc SPIE. 2002; 4682:344.10.1117/12.465575
3. Huang Y, Qu B, Sharma P, et al. Component Level Modular Design of a Solid State X-ray Image Intensifier for MxN Arrays. IEEE MIC. 2010; (M14-3)
4. [Last accessed on 4/6/2011.] http://www.e2v.com/products-and-services/high-performance-imaging-solutions/space---scientific-imaging/emccd-imaging-sensors---l3vision/

5. Madan SK, Bhaumik B, Vasi JM. Experimental observation of avalanche multiplication in charge-coupled devices. Electron Devices, IEEE Transactions on. Jun; 1983 30(6):694–699.10.1109/T-ED.1983.21191
6. Robbins MS, Hadwen BJ. The noise performance of electron multiplying charge-coupled devices. Electron Devices, IEEE Transactions on. May; 2003 50(5):1227–1232.10.1109/TED.2003.813462
7. Zhao W, Ristic G, Rowlands JA. X-ray imaging performance of structured cesium iodide scintillator. Med Phys. 2004; 31:2594–2605. [PubMed: 15487742]
8. [Last accessed on 4/6/2011.] http://incomusa.com/products-process/faceplates/materials/mlb57/
9. [Last accessed on 4/6/2011.] http://www.xilinx.com/support/documentation/data_sheets/ds312.pdf
10. [Last accessed on 4/6/2011.] http://sine.ni.com/nips/cds/view/p/lang/en/nid/202340
11. FOS - Fiber Optic Plate with Scintillator for Digital X-ray Imaging. Hamamatsu Corp; Bridgewater, NJ: 1996.
12. Kuhls-Gilcrist AT, Jain A, Bednarek DR, Rudin S. A Method for Measuring the MTF of Digital Radiography Systems Using Noise Response. Med Phys. 2009; 36(2766)10.1118/1.3182494
13. Kuhls-Gilcrist, AT.; Bednarek, DR.; Rudin, S. Component analysis of a new Solid State X-ray Image Intensifier (SSXII) using photon transfer and Instrumentation Noise Equivalent Exposure (INEE) measurements," SPIE vol. 7258, 2009. Proceedings from Medical Imaging 2009: Physics of Medical Imaging; Orlando, FL. p. 7258-42p. 725817p. 1-10.
14. [Last accessed on 4/6/2011] http://www.e2v.com/assets/media/files/documents/imaging-space-and-scientific-sensors/Papers/low_light_technical_note_1.pdf

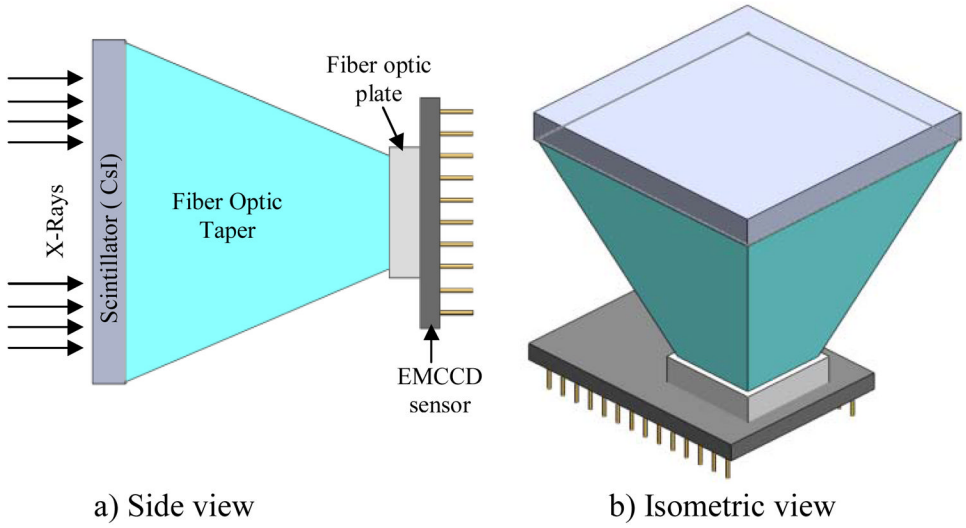

Fig 1.
EMCCD-based X-ray detector

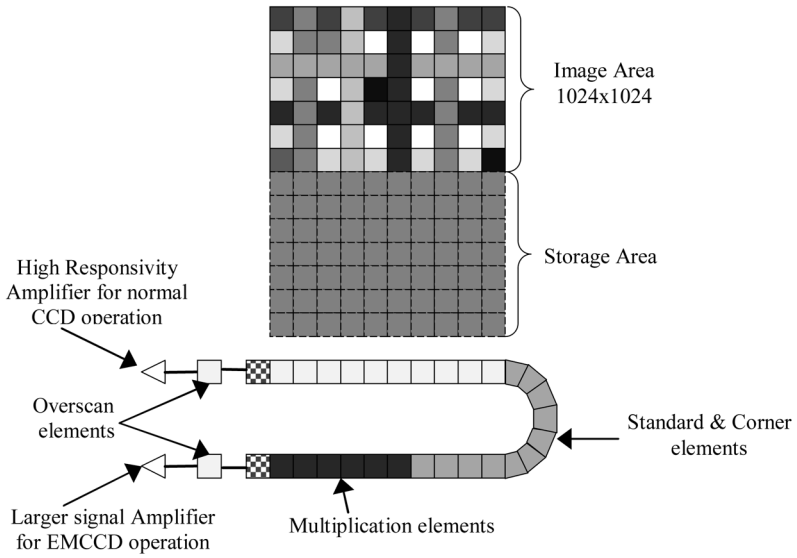

Fig. 2.
EMCCD sensor

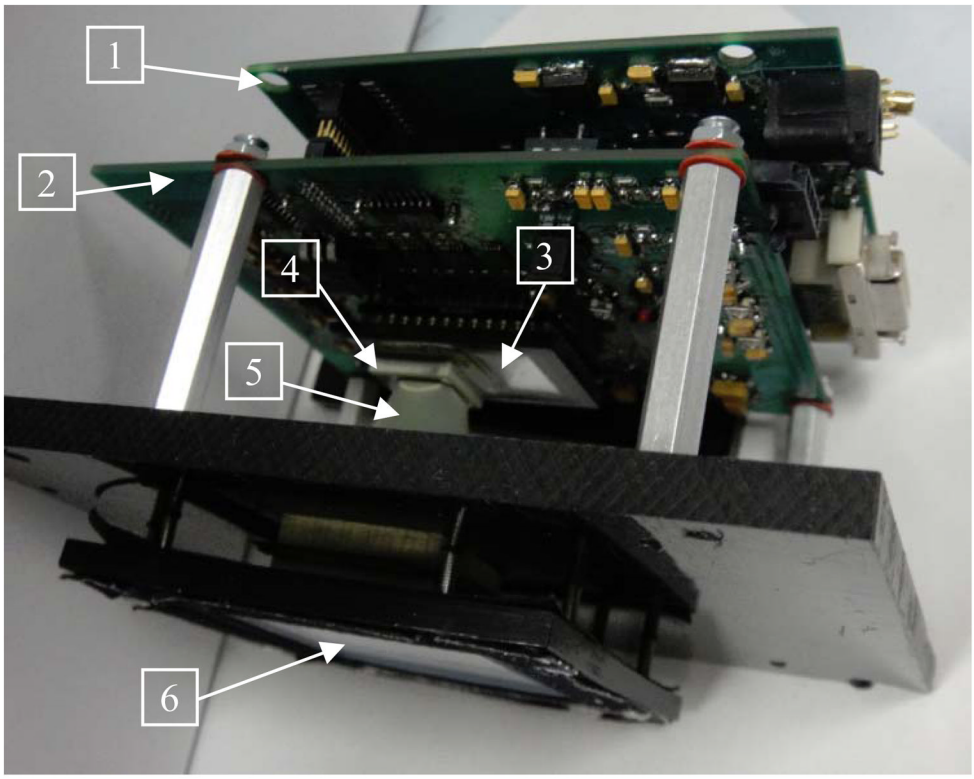

Fig 3.
Assembly for the prototype detector: (1) FPGA board (2) AFE board (3) EMCCD (4) FOP bonded to EMCCD (5) 3.3:1 FOT (6) CsI(TI)

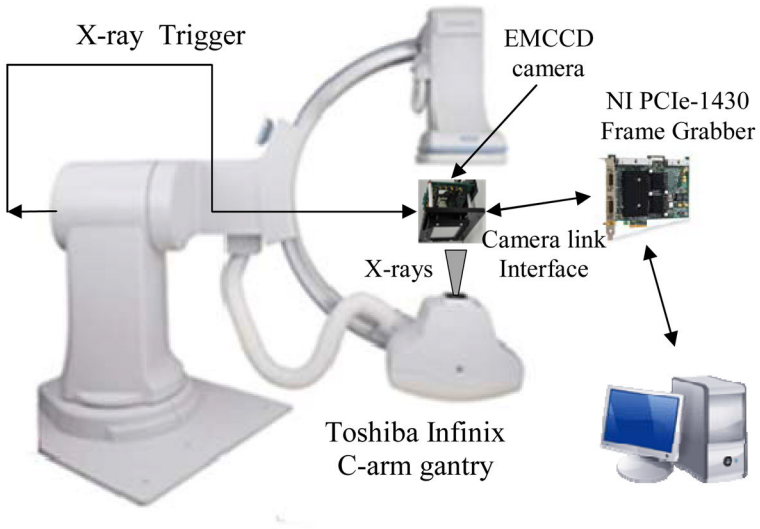

Fig. 4.
Functional Block Diagram for the prototype detector

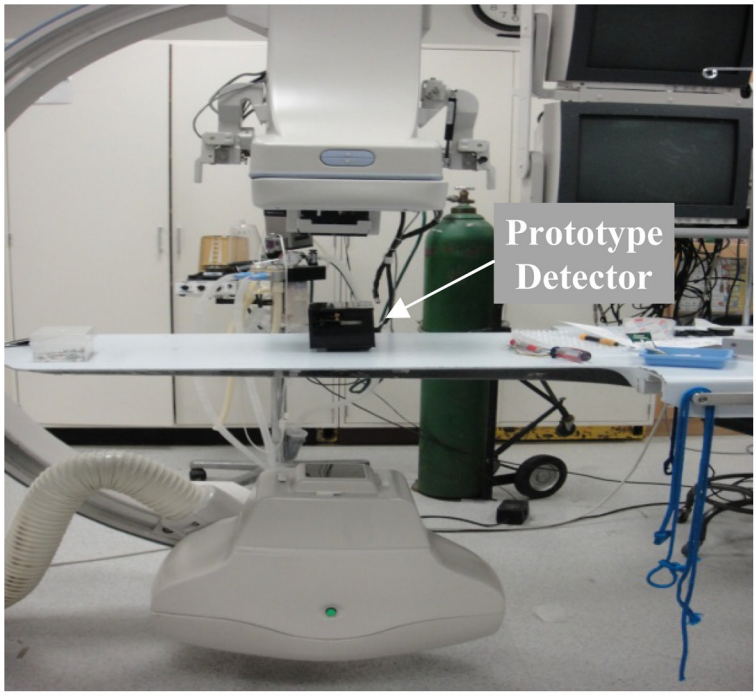

Fig 5.
Experimental setup for the prototype detector

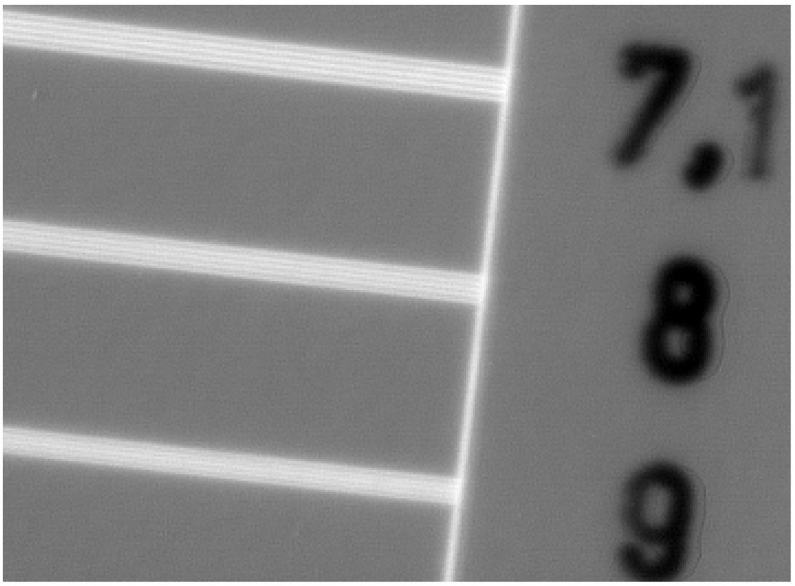

Fig 6.
X-ray image of a line pair phantom showing up to 9 line pairs/mm

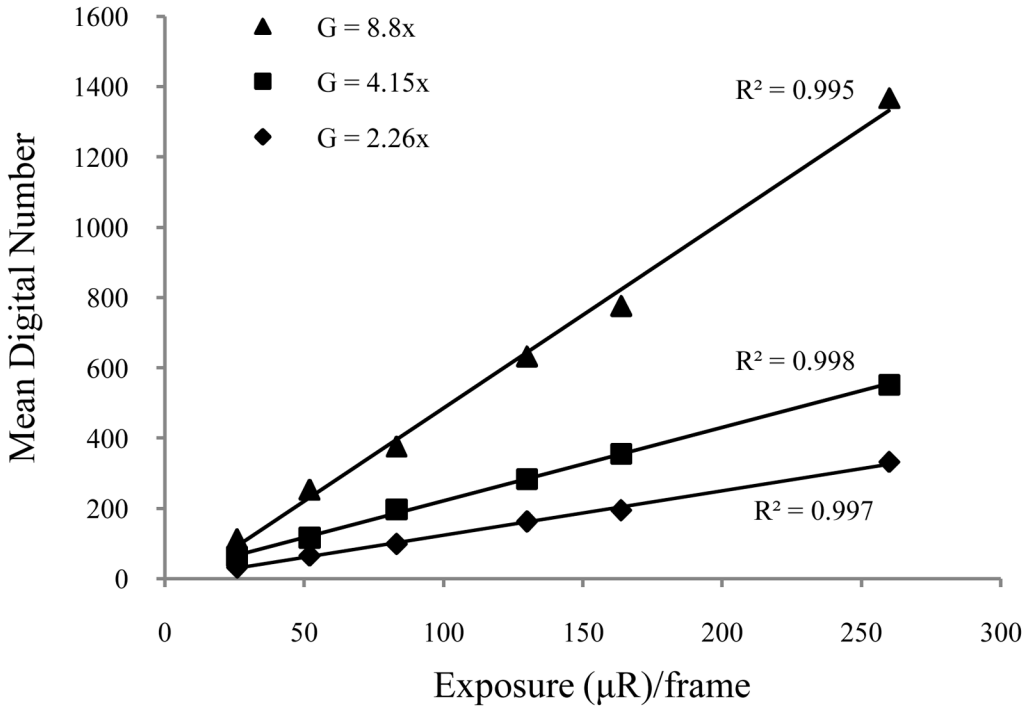

Fig. 7.
Detector linearity curves for different gains (G)

Fig 8(a) Gain =2x

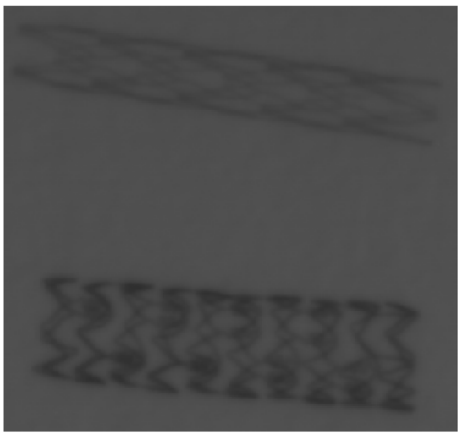

Fig 8(b) Gain =4x

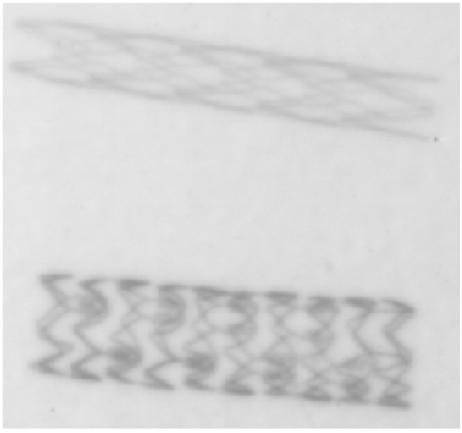

Fig 8(c) Gain =10x

Fig. 8.
Fig 8(a) Gain =2x
Fig 8(b) Gain =4x
Fig 8(c) Gain =10x

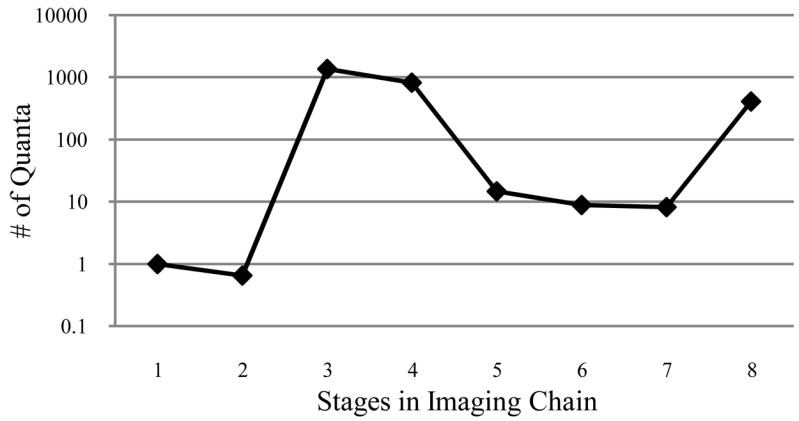

Fig. 9.
Quantum Accounting Diagram

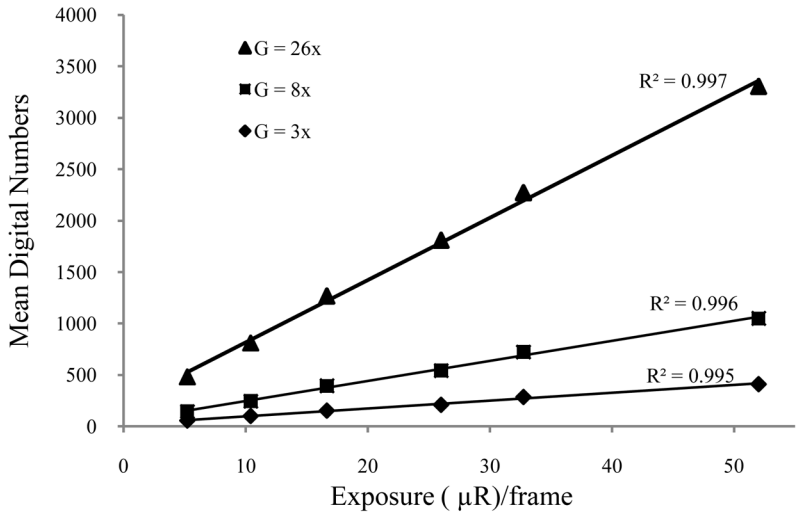

Fig. 10.
Detector linearity curves for different gains (G)